NASA Technical Memorandum 85851

Computation of Turbulent Flows Over a Backward-Facing Step

N.N. Mansour, J. Kim and P. Moin

October 1983

NASA
National Aeronautics and
Space Administration

NASA Technical Memorandum 85851

Computation of Turbulent Flows Over a Backward-Facing Step

N. N. Mansour, Stanford University, Stanford, California
J. Kim and P. Moin, Ames Research Center, Moffett Field, California

NASA
National Aeronautics and Space Administration

Ames Research Center
Moffett Field, California 94035

N84-12414

COMPUTATION OF TURBULENT FLOWS OVER A BACKWARD-FACING STEP*

N. N. MANSOUR‡
Stanford University, Stanford, California 94305

J. KIM and P. MOIN
NASA Ames Research Center, Moffett Field, California 94035

ABSTRACT

This paper presents a new numerical method for computing incompressible turbulent flows. The method is tested by calculating laminar recirculating flows and is applied in conjunction with a modified k-ϵ model to compute the flow over a backward-facing step. In the laminar regime, the computational results are in good agreement with the experimental data. The turbulent-flow study shows that the reattachment length is underpredicted by the standard k-ϵ model. The addition of a term to the standard model that accounts for the effects of rotation on turbulence improves the results in the recirculation region and increases the computed reattachment length.

NOMENCLATURE

A_x	$=\frac{1}{Re}\frac{\delta}{\delta x}\nu_e\frac{\delta}{\delta x}$, viscous operator in the x-direction
A_y	$=\frac{1}{Re}\frac{\delta}{\delta y}\nu_e\frac{\delta}{\delta y}$, viscous operator in the y-direction
C_p	pressure coefficient
C_μ	constant in the viscosity model (=0.09)
C_1, C_2	constants in the ϵ-equation(=1.44, 1.92)
C_3	constant for the rotation term in the ϵ-equation
D_x	convection and viscous operator in the x-direction
D_y	convection and viscous operator in the y-direction
f	flow quantity
h	step height
$\mathbf{H}$	block-diagonal matrix, defined in appendix
H_i	$=-\delta(u_iu_j)/\delta x_j$, differenced convective term
I	identity matrix

*Research supported by NASA Ames Research Center
‡ Present address: Sandia National Laboratories, Livermore, Calif. 94550.

k	$=\frac{1}{2}\overline{u'_j u'_j}$, turbulence kinetic energy
L_b	length of separation bubble
ℓ	$= C_\mu^{3/4} k^{3/2}/\epsilon$, dissipation length scale
N_x	number of grid points in the x-direction
N_y	number of grid points in the y-direction
$\mathbf{p}$	$=p/\rho + \frac{2}{3}k$
p	pressure
P_k	$=2\nu_T S_{ij} S_{ij}$, production term in k-equation
P_ϵ	$=C_1 \epsilon/k P_k$, production term in ϵ-equation
Re	$=Uh/\nu$, Reynolds number
$\mathbf{S}$	source term, defined in appendix
S_{ij}	$=\frac{1}{2}(\partial u_i/\partial x_j + \partial u_j/\partial x_i)$, strain-rate tensor
u_i	mean velocity component in the i-direction
u'_i	velocity fluctuation in the i-direction
U	maximum inlet velocity
x_r	reattachment length on *step* wall
x_4	separation point on *no-step* wall
x_5	reattachment point on *no-step* wall
$\partial/\partial x_i$	partial derivative operator
$\delta/\delta x_i$	partial differencing operator on a staggered grid
Δk	$= k^{n+1} - k^n$, time-increment of k
$\Delta \mathbf{q}$	increment vector
Δt	time-step ($=t^{n+1} - t^n$)
Δx	grid spacing in the x-direction
$\Delta \epsilon$	$= \epsilon^{n+1} - \epsilon^n$, time-increment of ϵ
ϵ	dissipation rate of k
ν	laminar kinematic viscosity
ν_e	$=1 + \nu_T$, effective kinematic viscosity
ν_T	turbulence kinematic viscosity
ρ	density
$\sigma_k, \sigma_\epsilon$	Prandtl numbers for k and ϵ (=1.0, 1.3)
τ_{ij}	$=-\overline{u'_i u'_j} + \frac{2}{3}k\delta_{ij}$, Reynolds stress
Φ	$=\mathbf{p} + O(\frac{\Delta t}{Re})$, scalar related to pressure
$\hat{\Phi}$	shifted cosine transform of Φ
Ω	$=(\frac{1}{2}\Omega_{ij}\Omega_{ij})^{1/2}$, rotation term
Ω_{ij}	$=\frac{1}{2}(\partial u_i/\partial x_j - \partial u_j/\partial x_i)$, rotation-rate tensor

Superscript

$*$	value evaluated at intermediate state
n	value evaluated at time-step $t^n = \sum_{i=1}^{n} \Delta t_i$

Subscript

$_{i,j}$ indicate direction i, j

$_{x,y}$ indicate direction x, y

1. INTRODUCTION

Recirculation bubbles are recurring problems in many flows of practical interest. The flow over a backward-facing step is an example of such flows. In this flow, the location of the separation point is fixed and the region where the flow reattaches can be isolated. One can then study the separation-reattachment process without any complexities resulting from motion of the separation point. It is this feature of the flow combined with the simplicity of its geometry that make it a prime candidate for both experimental and numerical investigations.

At the 1980–81 AFOSR-HTTM Stanford Conference on Complex Turbulent Flows, 11 groups using 15 methods computed the turbulent flow over a 2:3 sudden expansion (Eaton 1982). It was found that all the methods using the standard k-ϵ model underpredicted the reattachment length as measured by the experiment. These results indicate that a modification to the model is necessary. To test different models, an accurate numerical method should be used where no artificial viscosity is necessary to stabilize the solution.

One of the objectives of this paper is to present such a method for the incompressible Navier-Stokes equations. This method is used to test the effect of adding a rotation term to the k-ϵ turbulence model on predicting the flow over the 2:3 sudden expansion of Kim, Kline, and Johnston (1980). The particular method (developed in §3) uses central differencing on a staggered grid (Harlow and Welch 1965) in space and a partially implicit time-advancement algorithm combined with a direct Poisson solver to obtain a divergence-free velocity field at each time-step. Results for laminar and turbulent computations are presented in §4.

2. GOVERNING EQUATIONS

The Reynolds-averaged incompressible Navier-Stokes and continuity equations are

$$\frac{\partial}{\partial t}u_i + \frac{\partial}{\partial x_j}(u_i u_j) = -\frac{\partial}{\partial x_i}\mathrm{p} + \frac{1}{Re}\frac{\partial}{\partial x_j}(\tau_{ij} + 2S_{ij}) \tag{1}$$

$$\frac{\partial}{\partial x_i}u_i = 0 \tag{2}$$

Here, all the variables are nondimensionalized using the step height h and the maximum inlet velocity. All quantities not specifically defined in the text are defined in the nomenclature.

2.1 Turbulence Model

To close the above set of equations we need to express the Reynolds stresses, τ_{ij}, in terms of mean flow quantities. An eddy-viscosity model is used:

$$\tau_{ij} = 2\nu_T S_{ij} \tag{3}$$

where,

$$\frac{\nu_T}{Re} = C_\mu \frac{k^2}{\epsilon} \tag{4}$$

Here k is the turbulence kinetic energy and ϵ is the dissipation rate of k. The governing equations for k and ϵ can be derived from the equations of motion; they contain several terms that need to be modeled. The above eddy-viscosity model for τ_{ij} combined with the modeled equations for k and ϵ are known as the k-ϵ model (Jones and Launder 1972) . The high-Reynolds-number form of the k-ϵ model is known to produce poor results in the presence of rotation. Several modifications to the model are proposed in the literature to take into account the effects of rotation (Rodi 1979; Launder, Priddin, and Sharma 1977; Bardina, Ferziger, and Rogallo 1983). In this work, the term proposed by Bardina, Ferziger, and Rogallo(1983) to account for the effects of rotation is used in conjunction with the k-ϵ equations:

$$\frac{\partial}{\partial t}k + \frac{\partial}{\partial x_j}u_j k = P_k - \epsilon + \frac{1}{Re}\frac{\partial}{\partial x_j}\left(\frac{\nu_T}{\sigma_k}\frac{\partial}{\partial x_j}k\right) \tag{5}$$

$$\frac{\partial}{\partial t}\epsilon + \frac{\partial}{\partial x_j}u_j \epsilon = P_\epsilon - C_2\frac{\epsilon^2}{k} - C_3\Omega\epsilon + \frac{1}{Re}\frac{\partial}{\partial x_j}\left(\frac{\nu_T}{\sigma_\epsilon}\frac{\partial}{\partial x_j}\epsilon\right) \tag{6}$$

When $C_3 = 0$ is used, we refer to the model as the standard k-ϵ model. When $C_3 \neq 0$ we refer to the model as the modified k-ϵ model.

2.2 Boundary Conditions

To solve for the system of equations (1–6), boundary conditions are specified for all variables except pressure. With second-order differencing on a staggered grid, the continuity equation at the interior cells, together with the momentum equations at the interior grid points and the velocity boundary conditions, provides a closed system of algebraic equations for pressure (Moin 1982).

2.2.1 Inlet. All variables except pressure are prescribed at the inlet section. For the laminar cases, the streamwise velocity profile ($u(y)$) is taken to be parabolic. For the turbulent cases, the experimental profile (Kim, Kline, and Johnston 1980) for $u(y)$ at $x/h = 0$ is used. The k profile was set to $k = 3(\overline{u'^2} + \overline{v'^2})/4$ using the experimental values of $\overline{u'^2}$ and $\overline{v'^2}$ at $x/h = -1.33$. The inlet length scale was set

(Launder 1982) equal to $\ell = min\{2.5y, 0.5\delta\}$, where y is the distance to the wall and δ the boundary-layer thickness ($= 0.25h$).

2.2.2 Exit. All variables except pressure are extrapolated to the exit plane using $\partial f/\partial x = 0$.

2.2.3 Wall. At solid-wall boundaries, no-slip is used for the laminar cases. For turbulent cases, resolution restrictions, as well as the use of the high-Reynolds-number form of the k-ϵ model, require us to use near-wall submodels to bridge the gap between the wall and the first grid point away from the wall. In this model, the normal velocity component was set to zero at the wall. To specify the shear stress at the wall, we assume that the tangential velocity profile between the first grid point away from the wall and the wall is given by the law-of-the-wall (Kays 1966) as follows:

$$
\begin{aligned}
u^+ &= y^+ & y^+ &< 5 \\
u^+ &= -3.05 + 5 \ln y^+ & 5 < y^+ &< 30 \\
u^+ &= 5.5 + 2.5 \ln y^+ & 30 < y^+ &< (2000)
\end{aligned}
$$

where $u^+ = u/u^*$, and $y^+ = yu^*Re$. Then given u and y, we can find the value of u^* using the Newton iteration method. From the definition of u^* we have

$$\frac{\tau_{wall}}{\rho} = \frac{1}{Re}\frac{\partial u}{\partial y}\bigg|_{wall} = u^{*2}$$

The Neumann boundary condition, $\partial k/\partial n = 0$ was used for the k-equation. The dissipation equation at the cell center adjacent to the wall (point 2) was replaced by (Morel *et al.* 1981)

$$\epsilon_2 = C_\mu^{3/4}\left(\frac{k_2^{3/2}}{\ell_2}\right) \tag{7}$$

where the dissipation length scale ℓ_2 was obtained by interpolation, assuming that the dissipation length scale varies linearly between its value on the wall ($\ell_1 = 0$) and the value at the second cell away from the wall ($\ell_3 = \left(C_\mu^{3/4} k_3^{3/2}\right)/\epsilon_3$).

3. NUMERICAL METHOD

The equations of motion are discretized on a staggered grid uniform in the x-direction but not necessarily uniform in the y-direction. Central differencing is used to approximate the spatial derivatives. The velocities are defined on cell surfaces, while p, k and ϵ are defined at cell centers. The equations are then advanced in time using a fractional step method (Chorin 1968, Temam 1979) combined with the approximate-factorization technique (Douglas and Gunn 1964; Beam and Warming 1976; Briley and McDonald 1977).

3.1 Fractional Step

To advance the velocity field u_i from time-step n to n+1, the following time-discretization of the governing equations is used:

$$\frac{u_i^* - u_i^n}{\Delta t} = \frac{1}{2}(3H_i^n - H_i^{n-1}) + \frac{1}{2Re}\frac{\delta}{\delta x_j}\nu_e^n\left(\frac{\delta}{\delta x_j}u_i^* + \frac{\delta}{\delta x_j}u_i^n\right) \tag{8}$$

$$\frac{u_i^{n+1} - u_i^*}{\Delta t} = -\frac{\delta}{\delta x_i}\Phi^{n+1} \tag{9}$$

$$\frac{\delta}{\delta x_i}u_i^{n+1} = 0 \tag{10}$$

Note that the nonlinear terms are advanced by the second-order explicit Adams-Bashforth scheme, whereas the diffusion terms are advanced by the second-order Crank-Nicholson implicit scheme. Implicit treatment of the viscous terms eliminates the numerical viscous stability restriction. The inversion of eqn.(8) would require $O(N_x^2 N_y^2)$ operations (for $N_x = N_y$), and $O(N_x^2 N_y^2)$ words of memory; this would be costly. This problem is avoided by using an approximate-factorization method. The equations are first written in Δ-form:

$$(I - \frac{\Delta t}{2}A_x - \frac{\Delta t}{2}A_y)(u_i^* - u_i^n) = \Delta t\left(\frac{1}{2}(3H_i^n - H_i^{n-1}) + \frac{1}{Re}\frac{\delta}{\delta x_j}\nu_e^n\frac{\delta}{\delta x_j}u_i^n\right) \tag{11}$$

The left-hand side of (11) is then approximated as follows:

$$(I - \frac{\Delta t}{2}A_x)(I - \frac{\Delta t}{2}A_y)(u_i^* - u_i^n) = \Delta t\left(\frac{1}{2}(3H_i^n - H_i^{n-1}) + \frac{1}{Re}\frac{\delta}{\delta x_j}\nu_e^n\frac{\delta}{\delta x_j}u_i^n\right) \tag{12}$$

Note that eqn.(12) is an $O(\Delta t^3)$ approximation to eqn.(11). One proceeds by first solving a set of tridiagonal equations for $w_i = (I - \frac{\Delta t}{2}A_y)(u_i^* - u_i^n)$, and then for $(u_i^* - u_i^n)$. The solution of this system of equations requires $O(N_x N_y)$ operations, a significant reduction in cost.

3.2 Poisson Equation Solver

To update the velocity (u_i^{n+1}) using eqn.(9), Φ^{n+1} has to be determined.This is accomplished by applying the numerical divergence operator used in eqn.(10) to eqn.(9):

$$-\frac{\delta}{\delta x_i}\frac{\delta}{\delta x_i}\Phi^{n+1} = -\frac{1}{\Delta t}\frac{\delta}{\delta x_i}u_i^* \tag{13}$$

Poisson equations such as (13) are efficiently solved using transform methods. We first let (Williams 1969)

$$\Phi(i,j) = \sum_{l=0}^{N_x-2} \hat{\Phi}(l,j) \cos\left[\frac{\pi l}{N_x - 1}\left(i - \frac{3}{2}\right)\right], \tag{14}$$

for $i = 2,3,\ldots,N_x$, $j = 2,3,\ldots,N_y$. This cosine transformation will enforce a boundary condition for Φ consistent with the incompressibility condition and the velocity boundary conditions on staggered grids. Substituting eqn.(14) into eqn.(13) and using the orthogonality property of cosine, we obtain

$$k'_l \hat{\Phi}^{n+1} - \frac{\delta^2}{\delta y^2}\hat{\Phi}^{n+1} = -\frac{1}{\Delta t}\frac{\delta \hat{u}_i^*}{\delta x_i} \tag{15}$$

Here $k'_l = 2[1 - \cos(\frac{\pi l}{N_x - 1})]/\Delta x^2$ is the modified wave number, and Δx is the uniform grid spacing in the x-direction. The above tridiagonal system of equations can be inverted directly in the y-direction to yield $\hat{\Phi}^{n+1}$. Equation (14) is then used to compute Φ^{n+1}. The velocity is updated using eqn.(9). Note that $\mathbf{p} = \Phi + O(\frac{\Delta t}{Re})$, in the absence of variable eddy viscosity, i.e ν_e =constant, direct substitution yield $\mathbf{p} = \Phi + \frac{\nu_e \Delta t}{Re}\frac{\delta^2}{\delta x_j \delta x_j}\Phi$.

3.3 Update of Viscosity

In eqn.(8) the effective viscosity (ν_e) was lagged so that the k-ϵ equations were advanced separately. To integrate the k-ϵ equations in time, the approximate-factorization scheme in Δ-form was used. First the k-ϵ equations are approximated using a fully implicit Euler step:

$$\frac{\Delta k}{\Delta t} = C_\mu \frac{(k^{n+1})^2}{\epsilon^{n+1}}(2S_{ij}^{n+1}S_{ij}^{n+1}) - \epsilon^{n+1} - \frac{\delta}{\delta x_j}u_j^{n+1}k^{n+1} + \frac{1}{Re\sigma_k}\frac{\delta}{\delta x_j}\nu_T^n \frac{\delta}{\delta x_j}k^{n+1} \tag{16}$$

$$\frac{\Delta \epsilon}{\Delta t} = C_1 C_\mu k^{n+1}(2S_{ij}^{n+1}S_{ij}^{n+1}) - C_2\frac{(\epsilon^{n+1})^2}{k^{n+1}} - C_3\Omega^{n+1}\epsilon^{n+1} - \frac{\delta}{\delta x_j}u_j^{n+1}\epsilon^{n+1} + \frac{1}{Re\sigma_\epsilon}\frac{\delta}{\delta x_j}\nu_T^n\frac{\delta}{\delta x_j}\epsilon^{n+1} \tag{17}$$

where $\Delta k = k^{n+1} - k^n$, and $\Delta\epsilon = \epsilon^{n+1} - \epsilon^n$. The above equations are then linearized in time using Taylor series expansion about time-level n to give

$$(\mathbf{H} + \Delta t D_x + \Delta t D_y)\Delta \mathbf{q} = \Delta t \mathbf{S} \tag{18}$$

where

$$\Delta \mathbf{q} = \begin{pmatrix} \Delta k \\ \Delta \epsilon \end{pmatrix} \tag{19}$$

The block-diagonal matrix $\mathbf{H}$, and the block vector $\mathbf{S}$ are given in the appendix. The D_x and D_y terms are the convection-diffusion operators on a staggered grid in the x- and y-direction, respectively. For any reasonable number of grid points the inversion of eqn.(18) is prohibitively expensive. This problem is circumvented using factorization to approximate eqn.(18) as follows:

$$(\mathbf{H} + \Delta t D_x)\mathbf{H}^{-1}(\mathbf{H} + \Delta t D_y)\Delta \mathbf{q} = \Delta t \mathbf{S} \tag{20}$$

Equation(20) is an $O(\Delta t^3)$ approximation to eqn.(18). Two block tridiagonal matrix inversions and a matrix-vector multiplication will yield the solution to eqn.(20). Finally, k and ϵ are updated and the eddy viscosity is computed using eqn.(4).

4. RESULTS

The method described in §3 was used to simulate the flows over backward-facing steps in both laminar and turbulent regimes. The geometries of interest are those in which the channel walls are parallel so that the apparatus acts as a flow diffuser with strong adverse pressure gradient in the streamwise direction.

4.1 Laminar flow results. The laminar flow studied experimentally and numerically by Armaly *et al.* (1983) was chosen for this study. The particular geometry is a 1:2 sudden expansion with the inlet channel long enough so that the axial velocity profile at the step is parabolic. Computations were carried out using a 130 $\times$ 130 uniform grid for the Reynolds number (Re) range 100–800. The present results for the reattachment length[1], x_r, as a function of Re together with the experimental and numerical results of Armaly *et al.* are shown in Fig. 1. At $Re = 600$ the present results start to deviate from the experimental measurements. At this Reynolds number, mesh-refinement studies, as well as a check on the effect of the location of the exit boundary on the reattachment length, were carried out. From these investigations we conclude that the deviation from the experimental results is not due to numerical accuracy. A possible explanation for the deviation is that the experimental flow becomes three-dimensional at this Reynolds number (as Armaly *et al.* pointed out). Comparison with the numerical results of Armaly *et al.* shows that the present results, in the Reynolds number range 600–800, yield a much higher reattachment length than theirs.

Figure 2 shows the streamlines for $Re = 600$. Note the appearance of a recirculation bubble on the wall opposite the step. Unfortunately, no measurements are reported for $Re < 1000$ for this recirculation bubble. At $Re = 1000$, the first station where measurements are reported, the length of the bubble, $L_b (= x_5 - x_4)$,

[1]Defined as the point where the velocity changes sign.

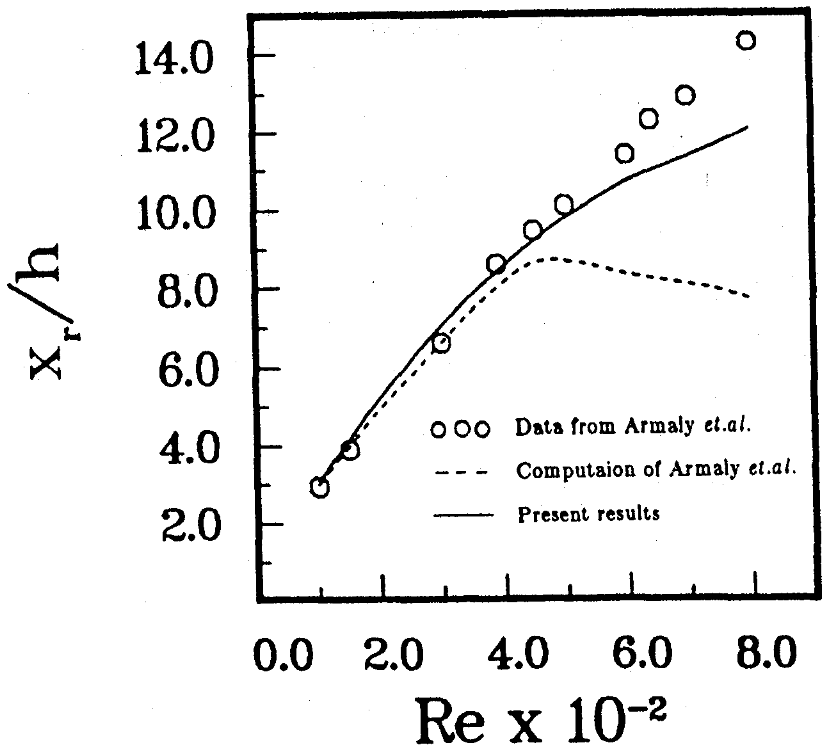

Figure 1. Reattachment length as a function of Reynolds number in the laminar range.

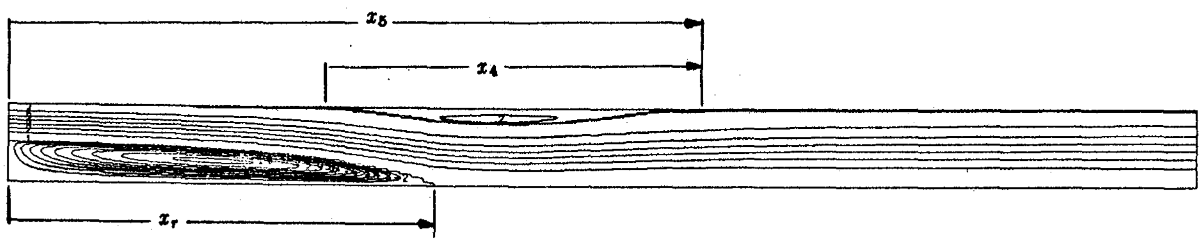

Figure 2. Streamlines at $Re = 600$: expansion ratio = 1:2.

is 10.4 step heights (h). For $Re > 1000$, the length of the experimentally observed bubble decreases with increasing Re. Our computations show that at $Re = 600$ the flow first separates on the *no-step* wall at $x_4 = 8.5h$, and reattaches at $x_5 = 16.3h$, resulting in a bubble length $L_b = 7.8h$. At $Re = 800$, we compute a bubble growth to $L_b = 11.5h$.

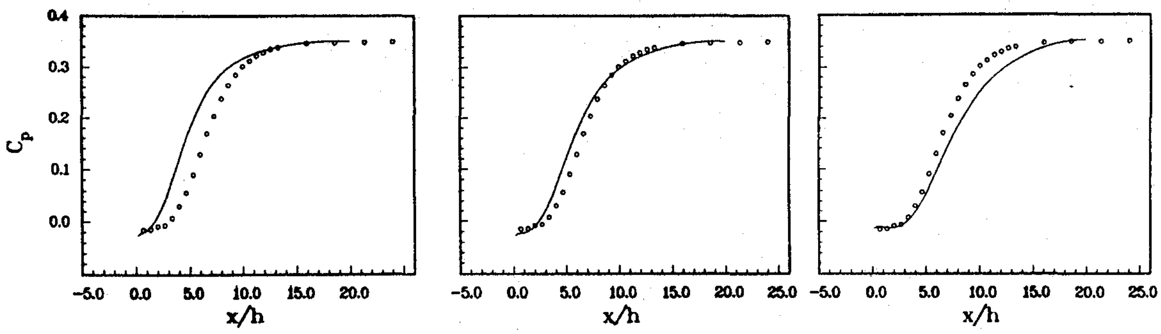

(a) Case 1, $C_3 = 0$. (b) Case 2, $C_3 = 0.075$. (c) Case 3, $C_3 = 0.15$.

Figure 3. Pressure distribution on the *no-step side* wall; symbols are the experimental data (Kim *et al.* 1980).

4.2 Turbulent Flow Results. At high Reynolds numbers, the flow over a backward-facing step becomes turbulent, and the mean flow in this regime exhibits one recirculation bubble behind the step. The turbulent flow selected for this study is the same as one of the flows selected for the 1980–81 AFOSR-HTTM Stanford Conference. The geometry is a 2:3 sudden-expansion (Kim, Kline, and Johnston 1980), and the Reynolds number at which extensive measurements are provided is $Re = 44,580$. When this flow was simulated by different groups using the standard k-ϵ model, it was found that the reattachment length is underpredicted by the model. Indeed, using the standard k-ϵ model and the boundary conditions prescribed in §2, we compute a reattachment length $x_r = 5.2h$. The reattachment length measured experimentally is about $x_r = 7h$, with an uncertainty of one step height. When we compare our numerical results for the pressure rise on the *no-step* wall with the experimental data (Fig. 3a), we find that a short reattachment length results in a shifted (with respect to the experimental data) pressure coefficient, C_p, profile.

These results suggest that a modification to the standard model is necessary. It is known that an additional term is needed in the ϵ-equation to account for the effects of rotation on the length scale (Launder *et al.* 1977). It is then not surprising that the large recirculation bubble present in the backward-facing step flows is mispredicted by the model. If we use the modified k-ϵ model (described in §2) with the constant recommended by Bardina *et al.* (1983) ($C_3 = 0.15$), we find that we overpredict the reattachment length, $x_r = 9.5h$. By increasing the reattachment length, the C_p profile shifts in the desired direction (Fig. 3c). However, by overpredicting x_r, the shift is too severe. One can then adjust C_3 to match closely the experimental reattachment length. We choose to use a constant equal to half the value recommended by Bardina *et al.* Fine tuning for a closer match was not necessary for the following reasons. Using $C_3 = 0.075$, the calculated reattachment length is $x_r = 6.6h$, resulting in good agreement with the data. However, if we are interested in the pressure rise on the step-side wall, we find that in all three cases, the calculated results underpredict the experimental curve in the range $x = 8$–$16h$ (Fig. 4). Fine tuning C_3 will not improve the results in this range.

In what follows we will refer to cases 1, 2, and 3 to indicate results obtained using $C_2 = 0.$, 0.075, and 0.15, respectively. With case 1, the effects of rotation as modeled by Bardina *et al.* are not included. Close examination of Fig. 4 shows that accounting for the effects of rotation, case 3, will result in good agreement with the experimental data in the range $x = 0$–$7h$. On the other hand, the recovery region ($x > 7h$) is poorly predicted. The reasons for the discrepancies can be better understood by comparing the calculated mean profiles with the experimental data.

Figures 5–7 show the mean-velocity profiles at $x = 5.3h$, $10.7h$, and $16h$ for the three cases. Clearly, in the recirculation region ($x < 7h$, Fig. 5) the maximum reverse velocity is best predicted with case 3, and is poorly predicted when the rotation term is not included (case 1). Case 2 yields the best overall agreement with

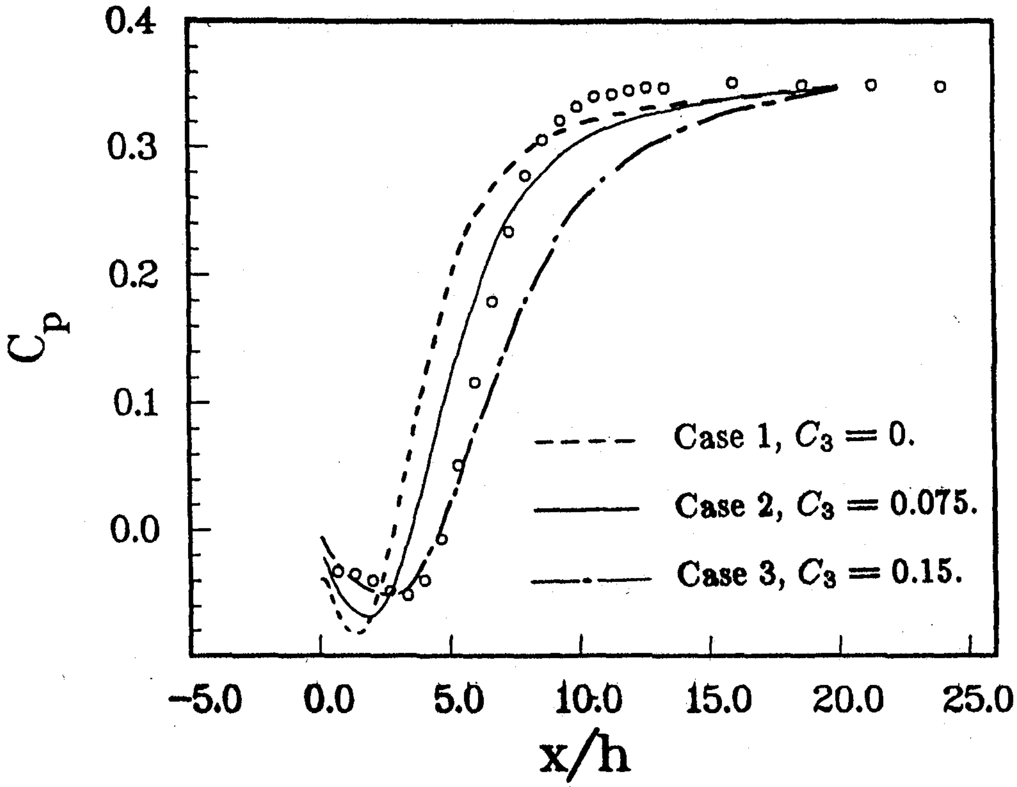

Figure 4. Pressure distribution on the *step side wall.* Symbols are the experimental data (Kim *et al.* 1980).

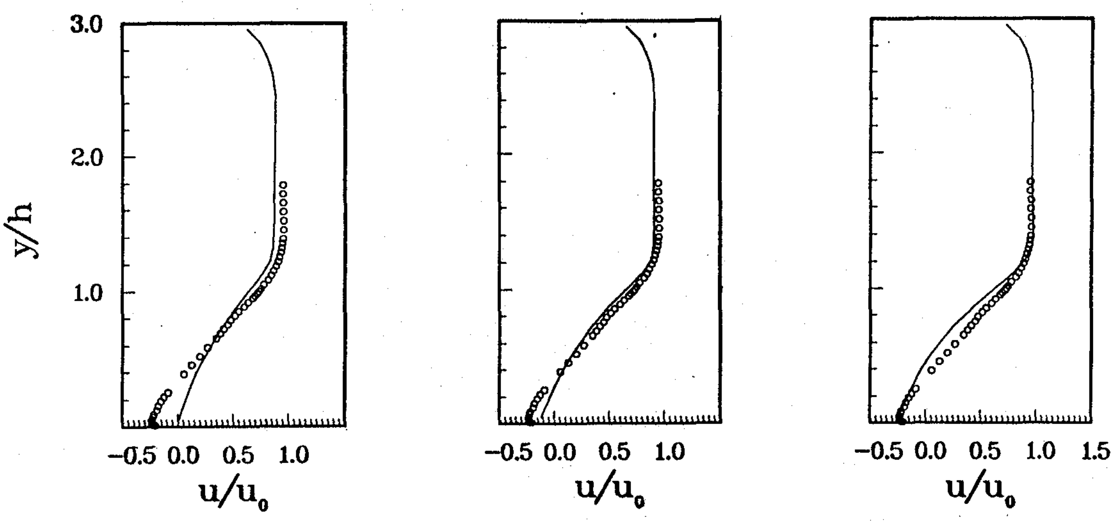

(a) Case 1, $C_3 = 0$. (b) Case 2, $C_3 = 0.075$. (c) Case 3, $C_3 = 0.15$.

Figure 5. Mean-velocity profiles at $x = 5.3h$; symbols are the experimental data (Kim *et al.* 1980).

the experimental data at $x = 5.3h$. The recovery of the mean profile (from one showing reverse flow to a fully developed channel flow profile) is not well predicted in all cases (Fig. 6 and 7). In all cases, the calculated recovery is slower than what

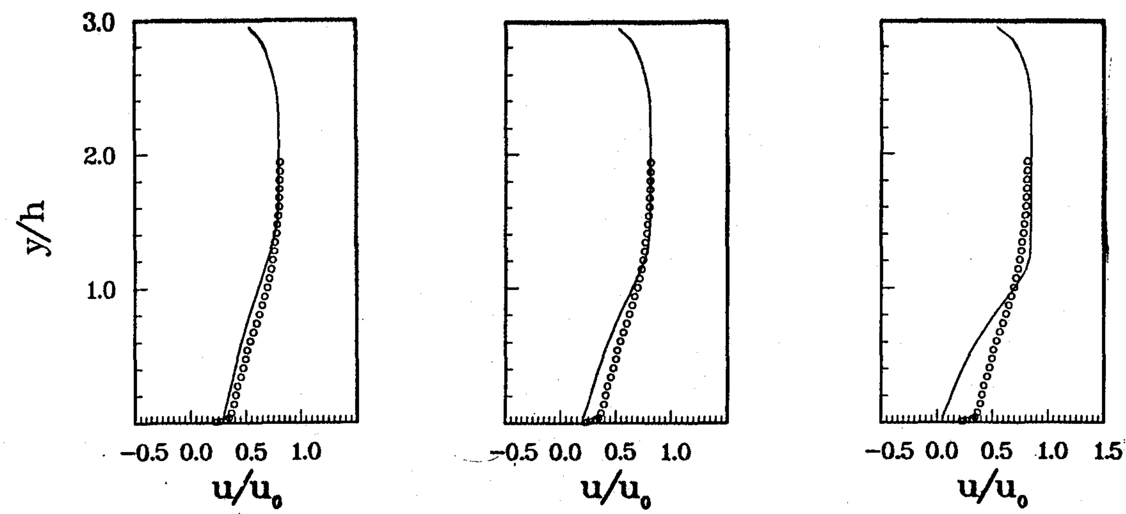

(a) Case 1, $C_3 = 0$. (b) Case 2, $C_3 = 0.075$. (c) Case 3, $C_3 = 0.15$.

Figure 6. Mean-velocity profiles at $x = 10.7h$; symbols are the experimental data (Kim *et al.* 1980).

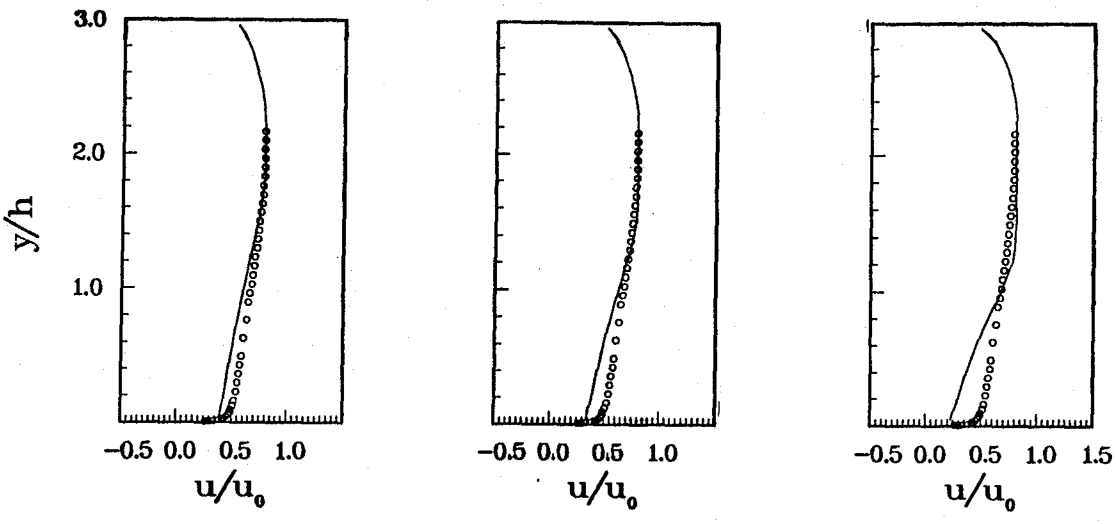

(a) Case 1, $C_3 = 0$. (b) Case 2, $C_3 = 0.075$. (c) Case 3, $C_3 = 0.15$.

Figure 7. Mean-velocity profiles at $x = 16h$. Symbols are the experimental data (Kim *et al.* 1980).

the experimental data indicate. The good agreement observed for case 1 at $x = 10.7h$ (Fig. 6a) is superficial. In case 1, a short reattachment length is calculated, so the recovery length at $x = 10.7h$, $L_r = 5.5h(= x - x_r)$, over which the profile was adjusting, is much longer than the recovery length over which the experimental profile adjusted ($L_r = 3.6h$). In other words, if we had used the reattachment point as the reference point, the mean profile would not show good agreement with the data.

The profiles of the turbulent kinetic energy and shear stress at three axial locations in the recovery region are shown with the experimental data for case 2 in Figs. 8 and 9. In general, the location of the peaks and the shape of the profiles are well predicted. However, the magnitudes are underpredicted, suggesting that the k-ϵ model underpredicts the magnitude of the dissipation length scale in the recovery region.

5. SUMMARY AND CONCLUSIONS

In this study, a numerical method for computing the incompressible Navier-Stokes equations has been developed. The method is time-accurate and the flow field satisfies the continuity equation up to machine accuracy at every time-step. The method was tested by calculating laminar recirculating flows and was applied in conjunction with a k-ϵ model to compute the turbulent flow over a 2:3 sudden expansion.

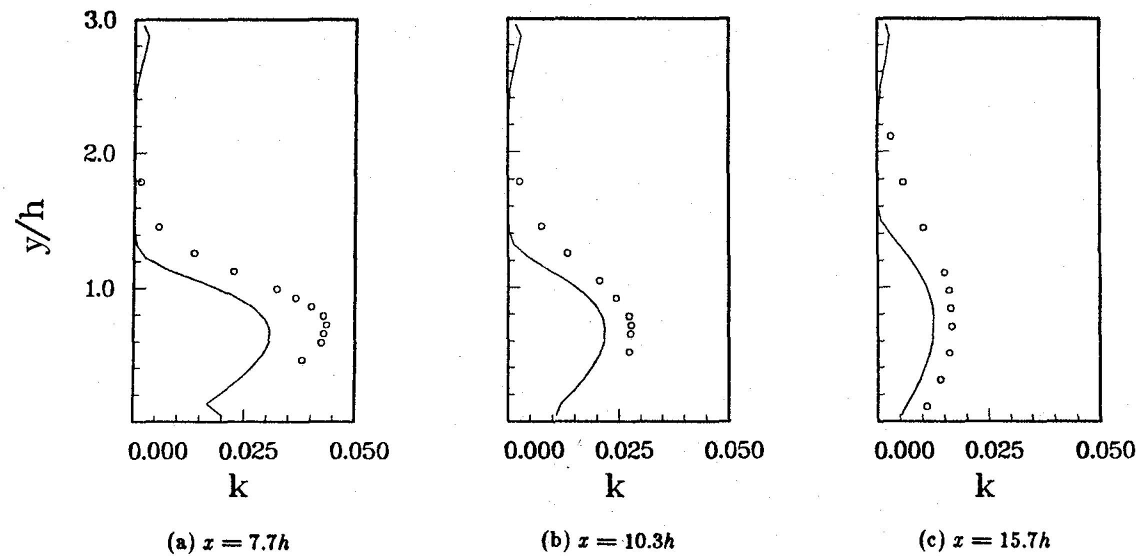

Figure 8. Turbulent kintetic energy profiles for case 2; symbols are the experimental data (Kim *et al.* 1980).

In the laminar regime the computational results are in good agreement with the data up to $Re = 500$. For $Re > 500$, the descrepancy between the computations and experiments is due to three-dimensionality in the experimental flow field. The turbulent flow study shows that the reattachment length is underpredicted by the

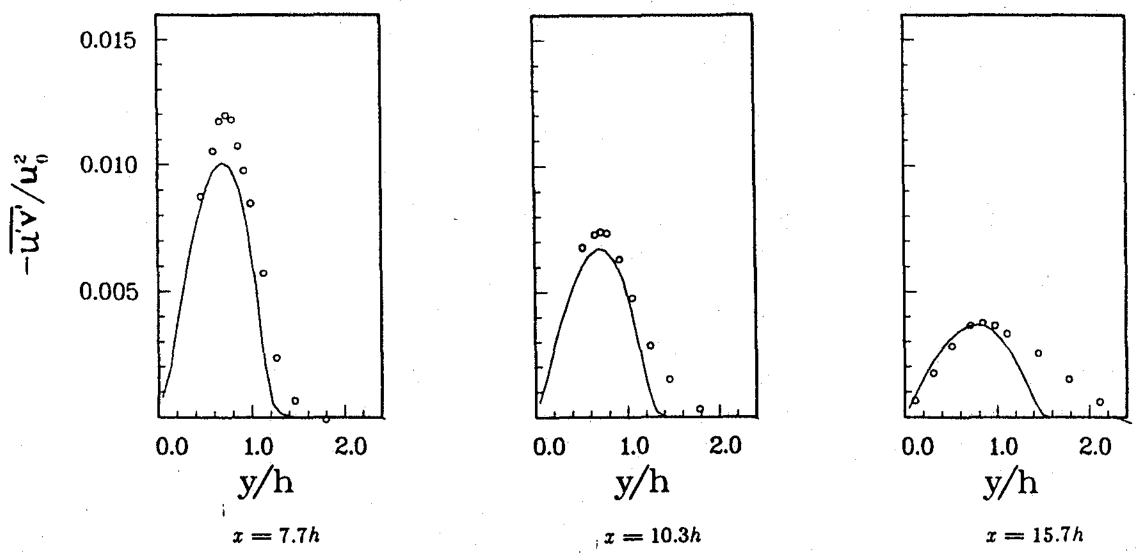

Figure 9. Turbulent shear stress profiles for case 2. Symbols are the experimental data (Kim *et al* 1980).

standard k-ϵ model. The addition of a term that accounts for the effect of rotation to the standard model improves the results in the recircultion region and increases the reattachment length. However, the recovery of the mean profiles is still not adequately predicted.

APPENDIX

The linearization of eqns.(16) and (17) using Taylor series expansions and dropping the terms $O(\Delta t^2)$ and higher yields:

$$\frac{\Delta k}{\Delta t} - C_\mu \frac{2k}{\epsilon}(2S_{ij}^{n+1}S_{ij}^{n+1})\Delta k + C_\mu \frac{k^2}{\epsilon^2}(2S_{ij}^{n+1}S_{ij}^{n+1})\Delta\epsilon + \Delta\epsilon - \frac{1}{Re\sigma_k}\frac{\delta}{\delta x_j}\nu_T\frac{\delta}{\delta x_j}\Delta k$$
$$+ \frac{\delta}{\delta x_j}u_j^{n+1}\Delta k = C_\mu\frac{k^2}{\epsilon}(2S_{ij}^{n+1}S_{ij}^{n+1}) - \epsilon + \frac{1}{Re\sigma_k}\frac{\delta}{\delta x_j}\nu_T\frac{\delta}{\delta x_j}k - \frac{\delta}{\delta x_j}u_j^{n+1}k \tag{A1}$$

$$\frac{\Delta\epsilon}{\Delta t} - C_1C_\mu(2S_{ij}^{n+1}S_{ij}^{n+1})\Delta k + 2C_2\frac{\epsilon}{k}\Delta\epsilon - C_2\frac{\epsilon^2}{k^2}\Delta k + C_3\Omega^{n+1}\Delta\epsilon$$
$$- \frac{1}{Re\sigma_\epsilon}\frac{\delta}{\delta x_j}\nu_T\frac{\delta}{\delta x_j}\Delta\epsilon + \frac{\delta}{\delta x_j}u_j^{n+1}\Delta\epsilon = C_1C_\mu k(2S_{ij}^{n+1}S_{ij}^{n+1}) - C_2\frac{\epsilon^2}{k} - C_3\Omega^{n+1}\epsilon$$
$$+ \frac{1}{Re\sigma_\epsilon}\frac{\delta}{\delta x_j}\nu_T\frac{\delta}{\delta x_j}\epsilon - \frac{\delta}{\delta x_j}u_j^{n+1}\epsilon \tag{A2}$$

All quantities without superscript are evaluated at time level n. Equations ($A1$) and ($A2$) are rearranged in the compact form of eqn.(18) where **H** is a block diagonal matrix with elements

$$\mathbf{H}_i = \begin{pmatrix} 1 - \Delta t C_\mu 2k(2S_{lm}^{n+1}S_{lm}^{n+1})/\epsilon & \Delta t(C_\mu k^2(2S_{lm}^{n+1}S_{lm}^{n+1})/\epsilon^2 + 1) \\ -\Delta t(C_1C_\mu(2S_{lm}^{n+1}S_{lm}^{n+1}) - C_2\epsilon^2/k^2) & 1 + \Delta t 2C_2\epsilon/k + C_3\Omega^{n+1} \end{pmatrix} \tag{A3}$$

and **S** is a block vector with elements

$$\mathbf{S}_i = \begin{pmatrix} C_\mu k^2(2S_{lm}^{n+1}S_{lm}^{n+1})/\epsilon - \epsilon - \frac{\delta}{\delta x_j}u_j^{n+1}k + \frac{1}{Re\sigma_k}\frac{\delta}{\delta x_j}\nu_T\frac{\delta}{\delta x_j}k \\ C_1C_\mu k(2S_{lm}^{n+1}S_{lm}^{n+1}) - C_2\epsilon^2/k - C_3\Omega^{n+1}\epsilon - \frac{\delta}{\delta x_j}u_j^{n+1}\epsilon + \frac{1}{Re\sigma_\epsilon}\frac{\delta}{\delta x_j}\nu_T\frac{\delta}{\delta x_j}\epsilon \end{pmatrix} \tag{A4}$$

REFERENCES

Armaly, B.F., Durst, F., Pereira, J.C.F., and Schönung, B.S., "*Experimental and Theoretical Investigation of Backward-Facing Step Flow,*" J.F.M, vol. 127, 1983, pp. 473–496.

Bardina, J., Ferziger, J.H. and Rogallo, R.S., "*Effect of Rotation on Isotropic Turbulence: Computation and Modeling,*" 1983, to be published.

Beam, R.M. and Warming, R.F., "*An Implicit Finite-Differenced Algorithm for Hyperbolic Systems in Conservation-Law Form,*" J. Comp. Phys., vol. 22, No. 1, 1976, pp. 87–110.

Briley, W.R. and McDonald, H., "*Solution of Multidimensional Compressible Navier-Stokes Equations by a General Implicit Method,*" J. Comp. Phys., vol. 24, No. 4, 1977, p. 428.

Chorin, A.J., "*Numerical Solution of the Navier-Stokes Equations,*" Mat. Comp., vol. 23, 1968, pp. 341–354.

Douglas, J. and Gunn, J.E., "*A General Formulation of Alternating Direction Methods,*" Numerische Math., vol. 6, 1964, p. 428.

Eaton, J.K., "*Incompressible Separated Flows—Internal Flows, Backward-Facing Step,*" 1980-81 AFOSR-HTTM Stanford Conf., *Complex Turbulent Flows*, Vol. II, Ed. S.J. Kline, B.J. Cantwell, G.M. Lilley, Thermosciences Div., Stanford University, 1982, pp. 886–904.

Harlow, F.H. and Welch, J.E., "*Numerical Calculation of Time-Dependent Viscous Incompressible Flow,*" Phys. Fluids, vol. 8, 1965, p. 2182.

Jones, W. P., and Launder, B. E., "*The Prediction of Laminarization with a Two-Equation Model of Turbulence,*" Int. J. Heat and Mass Transfer, vol. 15, 1972, p. 301.

Kays, W.M., *Convective Heat and Mass Transfer*, McGraw-Hill, 1966, New York.

Kim, J., Kline, S.J. and Johnston, J.P., "*Investigation of a Reattaching Turbulent Shear Layer: Flow over a Backward-Facing Step,*" J. Fluids Eng., ASME Trans., vol. 102, 1980, pp. 302–308.

Launder, B.E., "*Influence of Numerics and Computor Variance in the Computation of Complex Turbulent Flows,*" 1980-81 AFOSR-HTTM Stanford Conf., *Complex Turbulent Flows*, Vol. II, Ed. S.J. Kline, B.J. Cantwell, G.M. Lilley, Thermosciences Div., Stanford University, 1982, pp. 843–862.

Launder, B.E., Priddin, C.H., and Sharma, B.I., "*The Calculation of Turbulent Boundary Layers on Spinning and Curved Surfaces,*" J. Fluid Eng., ASME Trans., 1977, pp. 231–239.

Moin, P., "*Numerical Simulation of Wall-Bounded Turbulent Shear Flows,*" Proc. 8th International Conf. Num. Meth. Fluids Mech., Aachen, Ed. Krause, E., Notes in Physics, vol. 170, 1982, pp. 55–74.

Morel, T., Mansour, N.N., Saxena, V., and Rask, R.B., "*Comparison of Calculated and Measured Velocities for a Turbulent Swirling Flow Inside a Cylindrical Enclosure*," 3rd Symposium on Turbulent Shear Flows, University of California, Davis, 1981, pp. 5.9–5.14.

Rodi, W., "*Influence of Buoyancy and Rotation on Equations for the Turbulent Length Scale*," 2nd Symposium on Turbulent Shear Flows, 1979, Imperial College, London, pp. 10.37–10.42.

Temam, R., *Navier-Stokes Equations, Theory and Numerical Analysis*, 2nd ed., North-Holland Pub. Co., 1979, Amsterdam.

Williams, G.P., "*Numerical Integration of the Three-Dimensional Navier-Stokes Equations for Incompressible Flow*," J.F.M., vol. 37, 1969, pp. 727–750.